[Short title + Author Name - P&H title] 17 (2024) 105650

Contents lists available at ScienceDirect

Arabian Journal of Chemistry

journal homepage: www.ksu.edu.sa

Novel modified probiotic gold nanoparticles loaded with ginsenoside CK exerts an anti-inflammation effect *via* NF-κB/MAPK signaling pathways

Seunghyun Kim [a,1], Rongbo Wang [a,1], Sanjeevram Dhandapani [a], Kyungsu Kang [b], Ik-Hyun Cho [c,*], Yeon-Ju Kim [a,*]

[a] *Graduate School of Biotechnology, and College of Life Science, Kyung Hee University, Yongin 17104, Republic of Korea*
[b] *Natural Product Informatics Research Center, Korea Institute of Science and Technology, Gangneung, Gangwon-do 25451, Republic of Korea*
[c] *Department of Science in Korean Medicine and Brain Korea 21 Plus Program, Graduate School, Kyung Hee University, Seoul 02447, Republic of Korea*

ARTICLE INFO

Keywords:
Bifidobacterium
Ginsenoside compound K (CK)
Gold nanoparticles
Anti-inflammation
NF-κB/MAPK pathway

ABSTRACT

Background: Gold nanoparticles (AuNPs) exhibit promising potential as medical materials due to their high biocompatibility, tunable size and shape, and excellent drug delivery capabilities, among other unique physicochemical properties. Previous studies have indicated the remarkable anti-inflammatory activity of ginsenoside compound K (CK). However, the relatively low bioavailability of CK restricts its effective delivery and action within the biological system. Hence, exploring novel delivery methods based on gold nanoparticles emerges as a promising strategy to overcome these challenges in application, thereby enhancing the therapeutic effectiveness of CK.

Methods: Probiotic-mediated AuNPs were synthesized using gold salt and the lysates of *Bifidobacterium animalis* subsp. *lactis*. Then, CK was loaded with AuNPs to form *Bifidobacterium* CK AuNPs (Bifi-CKAuNPs). The anti-inflammatory activity of Bifi-CKAuNPs was evaluated *in vitro* using RAW 264.7 cells and *in vivo* using mice. The NF-κB/ mitogen-activated protein kinases (MAPK) pathway was investigated as a potential mechanism of action.

Results: In vitro experiments showed that Bifi-CKAuNPs inhibited the activation of reactive oxygen species and reduced the expression of iNOS, COX-2, and pro-inflammatory cytokines (IL-1β, IL-6, and TNF-α) in RAW 264.7 cells. *In vivo* experiments showed that Bifi-CKAuNPs significantly reduced inflammation in the lung, kidney, and liver tissues of mice without toxicity. The anti-inflammatory activity of Bifi-CKAuNPs was mediated through the inhibition of NF-κB/MAPK signal transduction, which is a well-known and critical pathway in the pathogenesis of inflammation.

Conclusion: We have successfully synthesized and characterized Bifi-AuNPs, demonstrating its potent anti-inflammatory activity both *in vitro* and *in vivo*. Our results indicated that the NF-κB/MAPK pathway might play a key role in the mechanism of action of Bifi-CKAuNPs. These findings underscored the significant potential of Bifi-CKAuNPs as a promising platform for drug delivery and anti-inflammatory therapy. The observed efficacy in both cellular and animal models, along with insights into the underlying molecular pathways, positions Bifi-CKAuNPs as a valuable candidate for advancing therapeutic strategies in the realm of inflammation management.

1. Introduction

Panax ginseng (P. ginseng) is a plant species that belongs to the Araliaceae family, and it has long been used as traditional herbal medicine in East Asian countries (Potenza et al., 2023). This plant is known for its extensive therapeutic applications, including anti-inflammatory, anticancer, antioxidant, antihypertensive, antidiabetic, and immune system modulation effects (Ahmad et al., 2023). In addition, recent findings indicate that *P. ginseng* has the potential to enhance health status through the modulation of inflammasome activity in diverse pathological contexts, including instances of viral infection and neurological dysfunction (Ratan et al., 2021). Ginsenosides are the important

* Corresponding authors.
E-mail addresses: ihcho@khu.ac.kr (I.-H. Cho), yeonjukim@khu.ac.kr (Y.-J. Kim).
[1] These authors contributed equally to the manuscript.

https://doi.org/10.1016/j.arabjc.2024.105650
Received 2 June 2023; Accepted 22 January 2024
Available online 24 January 2024

active ingredients of ginseng and are triterpene glycoside compounds (Zhou et al., 2022). They can be divided into protopanaxadiol group saponins (PPD type saponins), protopanaxatriol group saponins (PPT type saponins) and oleanane type. The differentiation between PPD and PPT is dictated by the positioning of their sugar moieties (Hou et al., 2021). PPD exhibits sugar moiety attached to the 3-position of the triterpene dammarane benzene ring, encompassing Rg3, Rd, Rc, Rb1, and Rb2 (Cong et al., 2023). Conversely, the sugar moiety of PPT are affixed to the 6-position of the triterpene dammarane ring, including Rg1, Rg2, Rh1, and Re (Sarhene et al., 2021). Compound K (CK; 20-O-D-glucopyranosyl-20(S)-protopanaxadiol) emerges as a metabolic end product of PPD-type ginsenosides during human metabolism, synthesized through the enzymatic activity of intestinal bacteria subsequent to ginseng ingestion (Sharma & Lee, 2020). Renowned for its reported superior pharmacological effects, CK has demonstrated efficacy against inflammation, tumors, aging, allergies, and diabetes (Guo et al., 2023). However, the permeation of CK through intestinal membranes is partially impeded, resulting in poor absorption within the body (Tam et al., 2023). Hence, the development of safe and effective drug delivery systems is imperative to enhance the targeted delivery of CK to specific tissues and organs, thereby augmenting its therapeutic efficacy.

Gold nanoparticles (AuNPs) exhibit unique advantages for drug delivery and medical diagnostics, positioning them as a favorable choice in various biomedical contexts (Falahati et al., 2020). One key advantage is their exceptional biocompatibility, making them more suitable for biomedical applications with minimal cytotoxicity (Kumari et al., 2023; Wang et al., 2023b). For example, in comparison to AuNPs, silver nanoparticles (AgNPs) exhibit higher toxicity, posing adverse effects on health, while the chemical inertness of gold ensures higher stability and lower toxicity of AuNPs (Lapresta-Fernández et al., 2012). The ease of surface modification allows precise control over their properties, facilitating tailored applications in drug delivery and imaging (Abdelkawi et al., 2023; Sadeghi et al., 2015). The superior optical properties of AuNPs, particularly the surface-enhanced Raman scattering effect, serve as powerful tools for medical diagnostics (Wen et al., 2022). Furthermore, the substantial drug loading capacity of gold nanoparticles stems from their expansive surface area, facilitating effective encapsulation of drug molecules (Hassan et al., 2022). The potential for targeted delivery is derived from the ease of surface modification, enabling the attachment of ligands for the specific recognition of target cells or tissues (Nejati et al., 2021). Research has indicated that AuNPs can detect the presence of antigens on cell surfaces by acting as drug carriers and through conjugation with drugs (Borse et al., 2020). Therefore, loading ginsenosides onto specially designed drug delivery systems holds considerable promise and significance in advancing their biomedical applications. Despite these advantages, the application of AuNPs as carriers for drug delivery still encounters multiple challenges, including the complexity and high cost of the synthesis process.

Nanoparticle biofabrication refers to the synthesis process utilizing the intrinsic biochemical pathways of microorganisms, plants, or other biological entities (Zhang et al., 2020). In contrast to chemical or physical synthesis methods, this approach eliminates the need for hazardous solvents, aligning with principles of ecological stewardship (Gavilán et al., 2023). Moreover, biogenic synthesis is conducted under comparatively mild conditions, presenting a substantial enhancement in efficiency as opposed to the elevated energy requirements and protracted durations associated with chemical or physical synthesis (Radulescu et al., 2023). With an increasing focus on health, the use of probiotics for synthesizing gold nanoparticles has garnered attention (Dhandapani et al., 2021). Probiotic strains can efficiently reduce gold ions to create biocompatible gold nanoparticles, offering a sustainable method for customizing their properties, especially for medical applications (Liu et al., 2020; Mikhailova, 2021; Sarani et al., 2024). Research involving the biofabrication of gold nanoparticles using probiotic strains isolated from Korean kimchi for photothermal therapy in cancer treatment suggests the feasibility of utilizing probiotics for synthesizing anticancer gold nanoparticles (Balusamy et al., 2022). However, the biogenic synthesis of nanoparticles using probiotics and exploring its applications in other domains remain active research areas, necessitating further studies to comprehensively understand the scalability of this approach.

In order to promote the innovation of AuNPs synthesis technology and develop a delivery system to improve the bioavailability of CK as an inflammatory therapeutic agent, this study utilized probiotics (i.e., *Bifidobacterium animalis* subsp. *lactis*) to biosynthesize ginsenoside CK-loaded AuNPs (Bifi-CKAuNPs). The anti-inflammatory activity of ginsenoside CK has been widely demonstrated, indicating that Bifi-CKAuNPs are expected to exhibit enhanced anti-inflammatory efficacy as nanocarriers through the synergistic effects produced by ginsenoside CK. The optimal conditions for the biosynthesis of Bifi-CKAuNPs were monitored using ultraviolet–visible (UV–vis) absorption spectroscopy, and the physicochemical properties of the biosynthesized Bifi-CKAuNPs were characterized. Experimental studies on Bifi-CKAuNPs *in vitro* and *in vivo* were conducted to further examine their anti-inflammatory activity and the potential mechanism.

2. Materials and methods

2.1. Chemicals and materials

The Man, Rogosa, and Sharpe (MRS) broth and agar were provided by BD Biosciences (Seoul, Korea). Hydrogen(III) tetrachloroaurate hydrate ($HAuCl_4{\cdot}3H_2O$, Au) and 3-(4,5-dimethyl-thiazol-2yl)-2,5-diphenyltetrazolium bromide (MTT) were provided by Thermo Fisher (Waltham, MA USA). CK (≥95 %) was provided by Ginseng Bank at Kyung Hee University (Yongin, Republic of Korea).

2.2. Phylogenetic tree construction

The *B. animalis* subsp. *lactis* strain was obtained by incubating the isolated colony in MRS broth containing 0.5 g/L of L-Cysteine hydrochloride at 37 °C for 48 h. The obtained bacterium was sequenced, and its NCBI accession number was CP001606. 16S rRNA gene sequences were analyzed for the *B. animalis* subsp. *lactis* strain. Associated taxa were collected in the GenBank database using MEGA X, the phylogenetic tree was summarized using Ez Bio-Edit (Fig. S1).

2.3. Loading optimization of CK on AuNPs using the bacterial cell lysate

First optimize the synthesis conditions of nanoparticles. Different gold nanoparticles were obtained by changing the parameters such as bacterial biomass (OD: 0.2–1.0), gold salt concentration (0.5–2.5 mM), CK concentration (0.1–0.4 mM) and reaction pH (3–7), respectively. The optimized reaction conditions were selected depending on the highest absorbance peak. The final biosynthesis reaction was conducted as follows: incorporate a solution containing 2 mM $HAuCl_4{\cdot}_3H_2O$ and 0.3 mM CK into a 10 mL of the *B. animalis* subsp. *lactis*. biomass (OD_{600} = 1.0) solution. Then, the pH of the solution was adjusted to 7.0, and the solution was incubated at 37 °C for 24 h. The formation of nanoparticles (Bifi-CKAuNPs) was indicated by a change in the color of the reaction solution to purple. After the reaction, the nanoparticles were collected by centrifugation at 13,500 rpm for 20 min, during which they were washed three times with distilled water. Then, the synthesized nanoparticles were air-dried and used in subsequent experiments. The final yield of the nanoparticle was 7.502 mg/mL which was caculated according to the previously study (Sreedharan et al., 2019).

2.4. Characterization of Bifi-CKAuNPs

Physicochemical characterizations were performed on the Bifi-CKAuNPs. The absorption spectra (400–700 nm) of the nanoparticle solutions were obtained using an UV–vis spectrophotometer.

Additionally, Fourier transform infrared (FT-IR, PerkinElmer Inc., Waltham, MA, USA) spectroscopy, field emission transmission electron microscopy (FE-TEM, JEM-2100F), biological transmission electron microscopy (Bio-TEM, Talos L120C), and X-ray diffraction (XRD, D8 Advance, Bruker, Karlsruhe, Germany) were employed to determine the shape, size, and lattice characteristics of the synthesized nanoparticles. Dynamic light scattering (DLS, Otsuka Electronics, Shiga, Japan) particle analyzer was used to determine the size, stability, and dispersal nature of the nanoparticles.

2.5. Cell lines

Human keratinocytes (HaCaTs) were purchased from the American Type Culture Collection (Manassas, VA, USA). Mouse leukemic macrophages (RAW 264.7) and normal human dermal fibroblasts (NHDF) were purchased from the Korean Cell Line Bank (Seoul, Korea).

2.6. Cell viability test

The cytotoxicity of Bifi-CKAuNPs was investigated by performing an MTT assay according to the report by Awasthi *et al.* (Awasthi et al., 2021) to test the cytotoxicity of Bifi-CKAuNPs. Cells were individually seeded into 96-well plates at a density of 1×10^5 cells/well and incubated overnight. Prepared cells were treated with different concentrations of Bifi-CKAuNPs and cultured. After 24 h, 0.05 % MTT reagent was used to detect cell viability. Finally, optical density was recorded at 560 nm using a SpectraMax ABS Plus microplate reader (Sunnyvale, CA, USA), and the cell viability value was calculated.

2.7. Nitric oxide (NO) analysis

RAW 264.7 cells were seeded in 96-well culture plates at a density of 1×10^5 cells/well. After overnight incubation, LPS (1 μg/μL) was administered to the cells along with Bifi-CKAuNPs (20–60 μg/mL). After incubation for 24 h, the absorbance was measured at 570 nm, and the nitrite concentration was calculated using the $NaNO_2$ standard calibration curve.

2.8. Transmission electron microscopy analysis

RAW 264.7 cells were treated with Bifi-CKAuNPs (60 μg/mL). After 6 h, the cells were washed with phosphate-buffered saline and fixed with 2.5 % glutaraldehyde for 12 h. Cell pellets were sectioned using an ultramicrotome and stained with 3 % uranyl acetate and lead citrate. Finally, TEM imaging was performed using 80 kV JEM-1010 (JEOL, Tokyo, Japan).

2.9. 9. Quantitative real-time PCR analysis

LPS-stimulated RAW 264.7 cells were treated with Bifi-CKAuNPs. After 24 h, the mRNA of cells was extracted using TRIzol, and then the RT PreMix kit (Bioneer, Daejeon, Korea) was used to synthesize cDNA. Subsequently, qRT-PCR was performed to detect mRNA expression levels. The sequences of the primers are described in Table S1.

2.10. Western blot analysis

RAW 264.7 cells were cultured at a concentration of 5×10^5 cells/well for 24 h. Then they were treated with Bifi-CKAuNPs (20–60 μg/mL) and LPS (1 μg/mL) for 24 h. A radioimmunoprecipitation assay buffer was used to treat cells to obtain protein. Western blot analysis was performed according to a previous work for *in vivo* studies. The primary and secondary antibodies used in the experiments were provided by Abcam (Cambridge, UK). Immunoreactive bands were visualized using a chemiluminescent detection system (LAS-4000; Fujifilm, Tokyo, Japan) and normalized to Glyceraldehyde 3-phosphate dehydrogenase (GAPDH) on the same membrane.

2.11. Animals and ethical approval

Thirty-three male C57BL/6 mice (8 weeks old: body weight 22–23 g; Narabiotec Co., Ltd., Seoul, Korea) were used for the *in vivo* study of the effect of Bifi-CKAuNPs. The mice were maintained at a constant temperature of 23 ± 2 °C and humidity of 50 ± 10 % with a 12-h light–dark cycle. All experimental procedures were reviewed and approved by the Kyung Hee University Institutional Animal Care and Use Committee. During the study, the experimental animals were blinded for appropriate randomization and data processing according to the latest recommendations of the NIH Workshop on Preclinical Models of Neurological Disorders (Choi et al., 2018).

2.12. Experimental groups in mice

The mice were randomly divided into eight groups (n = 3). The sham group (n = 3) received distilled water *via* oral gavage for 3 days and intraperitoneal (i.p.) injection of physiological saline for 3 days. The LPS group (n = 3) received distilled water *via* oral gavage for 3 days and an i.p. injection of LPS (5 mg/kg) dissolved in physiological saline for 3 days. The Bifi-CKAuNPs + LPS group received Bifi-CKAuNPs (2.5, 5, and 10 mg/kg/day) *via* oral gavage for 3 days and an i.p. injection of LPS 3 days followed by the Bifi-CKAuNPs treatment. The CK + LPS group received CK (2.5, 5, and 10 mg/kg/day) *via* oral gavage for 3 days and an i.p. injection of LPS 3 days followed by the CK treatment.

2.13. Histopathological examination

To examine histopathological changes, the right lobe of the lung, median lobe of the liver, and right kidney from mice in each group were dissected, sliced, and fixed in a 4 % paraformaldehyde solution. The fixed slices were dehydrated using a standard-graded alcohol process, embedded in paraffin, and sectioned to reveal the overall structure of the organs. The paraffin sections were stained with hematoxylin & eosin (H&E). The severity of inflammation was ascertained using Microscope Imaging Software (National Institutes of Health, MD, USA) connected to a light microscope (BX40, Olympus Optical Co. Ltd., Tokyo, Japan).

2.14. Data analysis

The Inhibitory concentration (IC_{50}) were determined using GraphPad Prism 8 (GraphPad Software, La Jolla, CA). The severity of inflammation was determined *in vivo* using Microscope Imaging Software (National Institutes of Health, Maryland, USA) using the data obtained from the light microscope (BX40, Olympus Optical Co. Ltd., Tokyo, Japan). This analysis was performed as previsoluly reported. All experiments were performed in triplicate, and data were expressed as the mean ± standard error (SE). The statistical differences among means were analyzed by performing t-tests using Graph-Pad. Significant values were indicated as $^{*}p < 0.05$, $^{**}p < 0.01$, and $^{***}p < 0.001$. Student's *t*-test and ANOVA were performed using SPSS 21.0 (SPSS Inc, Chicago, IL, USA) (Amini et al., 2023; Marsousi et al., 2019).

3. Results and discussion

3.1. Optimization and characterization of biosynthesized AuNPs

Optimizing the conditions for nanoparticle synthesis is imperative for enhancing the reliability and reproducibility of reactions. Nanoparticles manifest surface plasmon resonance (SPR), a phenomenon involving the absorption and scattering of light within the UV–visible range. The peak height serves as an indicator of the intensity of this SPR. Alterations in nanoparticle size and concentration lead to corresponding changes in the position and intensity of the surface plasmon resonance

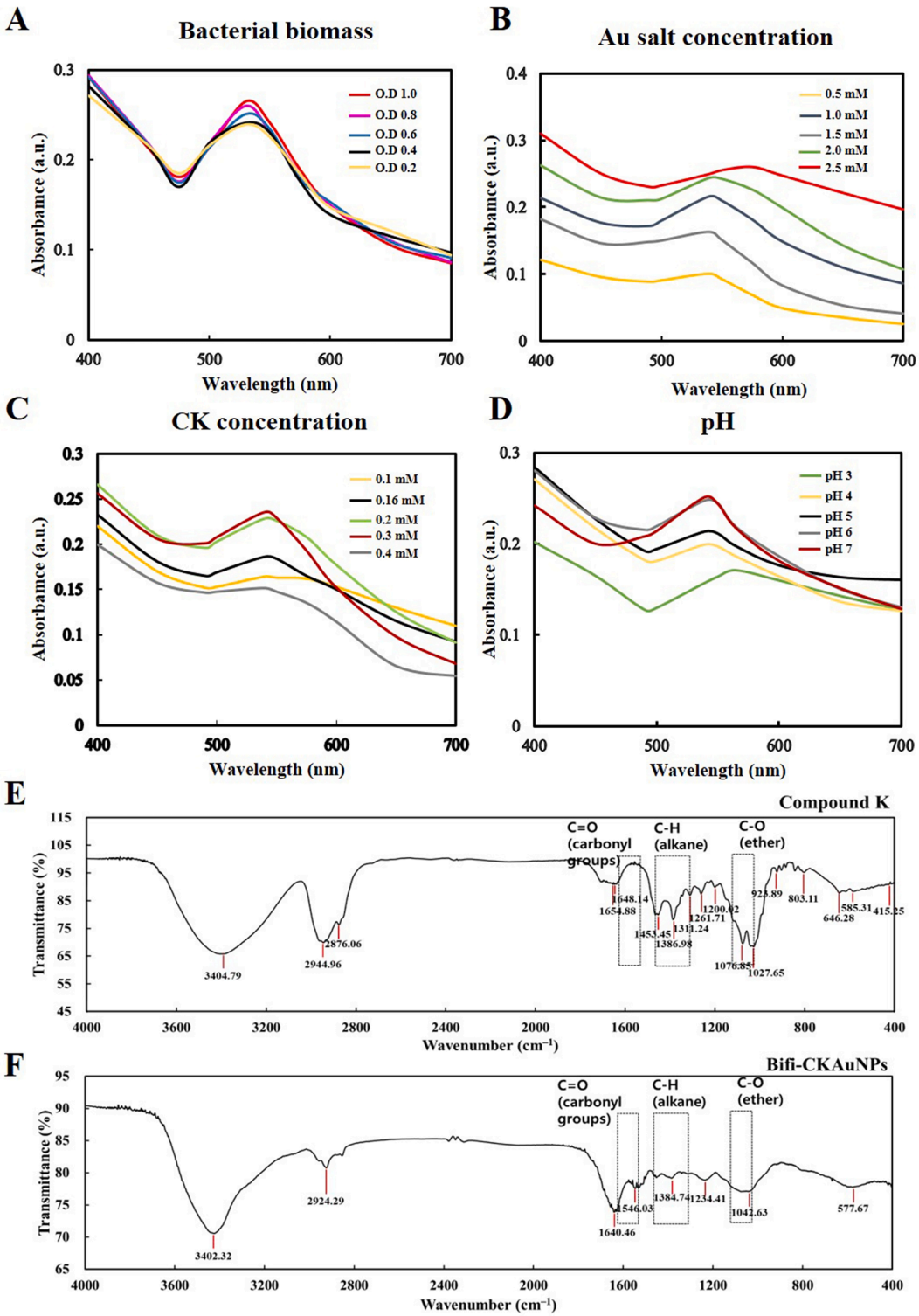

Fig. 1. Optimization and characterization of Bifi-CKAuNPs. Optimization of synthesized nanoparticles for each condition (turbidity of **A.** bacteria biomass, **B.** Au salt, **C.** concentration of CK and **D.** pH); FT-IR spectra of the **E.** CK, and **F.** Bifi-CKAuNPs.

peak (Paul et al., 2023). Generally, smaller AuNPs typically exhibit red, while larger ones may appear blue or purple hues (Yu et al., 2018; Zeng et al., 2020; Zou et al., 2018). Furthermore, the peak height demonstrates a proportional relationship with the concentration of nanoparticles. Increased nanoparticle concentration results in a heightened absorption signal, elevating the peak (Hammami & Alabdallah, 2021). Elevated peaks may signify a higher conversion in the synthesis reaction, whereas lower peaks may indicate diminished efficiency or the persistence of unreacted precursor species. Adhering to these principles, various nanoparticles were synthesized by manipulating bacterial biomass, Au salt concentration, CK concentration, and reaction pH conditions. Subsequently, the resulting gold nanoparticles were characterized using UV–visible spectroscopy to determine optimal conditions for the synthesis of CK-loaded AuNPs by regarding to the scrutiny of measured peaks. As shown in Fig. 1A-D, the optimal synthesis conditions that produced the highest peaks were bacterial growth (O.D:

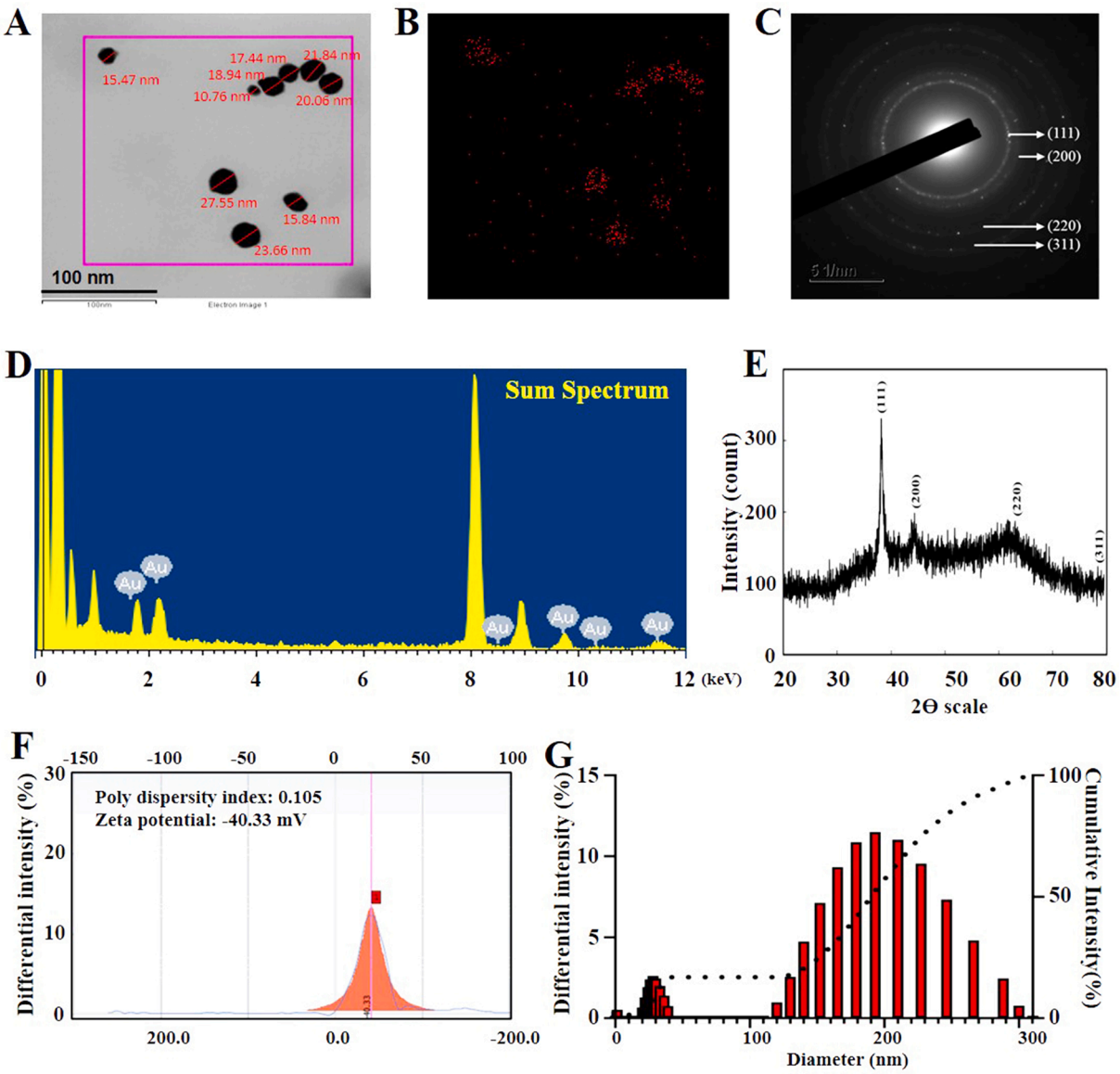

Fig. 2. **A**. Shape and size of Bifi-CKAuNPs; **B.** Gold distribution of Bifi-CKAuNPs **C**. SAED pattern of Bifi-CKAuNPs; **D.** EDX pattern of Bifi-CKAuNPs; **E.** XRD analysis of Bifi-CKAuNPs; **F**. Zeta-potential of Bifi-CKAuNPs; **G.** DLS analysis of Bifi-CKAuNPs size distribution.

1.0), gold salt (2.0 mM), CK concentration (0.3 mM), and pH (7). These optimized conditions were then used for the subsequent synthesis of Bifi-CKAuNPs.

Characterizing nanoparticles is crucial for understanding their physical, chemical, and biological properties, providing valuable insights into size, shape, stability, surface charge, and composition. These factors influence the behavior and performance of nanoparticles in various applications. The properties of Bifi-CKAuNPs were analyzed using different techniques. Firstly, the FTIR technique was employed to analyze the chemical bonds involved in the synthesis process. Fig. 1E and F show that the main chemical bonds identified were C = O (carbonyl group), C-H (alkane), and C-O ether, according to the spectrum library. And the detailed peak shifts were shown in Table S2. Taken together, these findings and peak changes indicate that CK was successfully loaded on newly synthesized Bifi-CKAuNPs.

Subsequently, we used TEM imaging to determine the shape of the synthesized nanoparticles (Fig. 2A). The Bifi-CKAuNPs exhibited spherical nanoparticles with sizes ranging from 10 to 25 nm, confirming their nanoscale dimensions. This indicates that the dimensions of Bifi-CKAuNPs are relatively small, suggesting potential advantages in biomedical applications such as superior drug delivery efficiency, cellular uptake capabilities, and biocompatibility (Sanità et al., 2020). It is well-established that nanoparticles possess the potential for recognition and clearance by the mononuclear phagocyte system (MPS) (Mills et al., 2022). Notably, the nanoparticles synthesized in this study exhibit a diminutive size, suggesting a heightened potential for evading engulfment by mononuclear phagocytes. The reduced dimensions of these nanoparticles imply an extended circulatory half-life within biological systems, facilitating efficient traversal across tissues and vascular barriers (Wang et al., 2023a). This characteristic may contribute to a deceleration in the recognition and clearance processes orchestrated by the MPS, consequently prolonging the residence time of the nanoparticles *in vivo*. It is imperative to underscore that further empirical investigations are necessary to validate these observations, and due consideration should be given to additional factors such as surface properties and biocompatibility (Huang et al., 2023a; Shen et al., 2023).

As shown in Fig. 2B, the presence of the Au element was verified through the elementary mapping, and the red color was the detected singal of the gold element. The SAED pattern (Fig. 2C) confirmed the crystalline structure with identified lattice planes (111, 200, 220, and

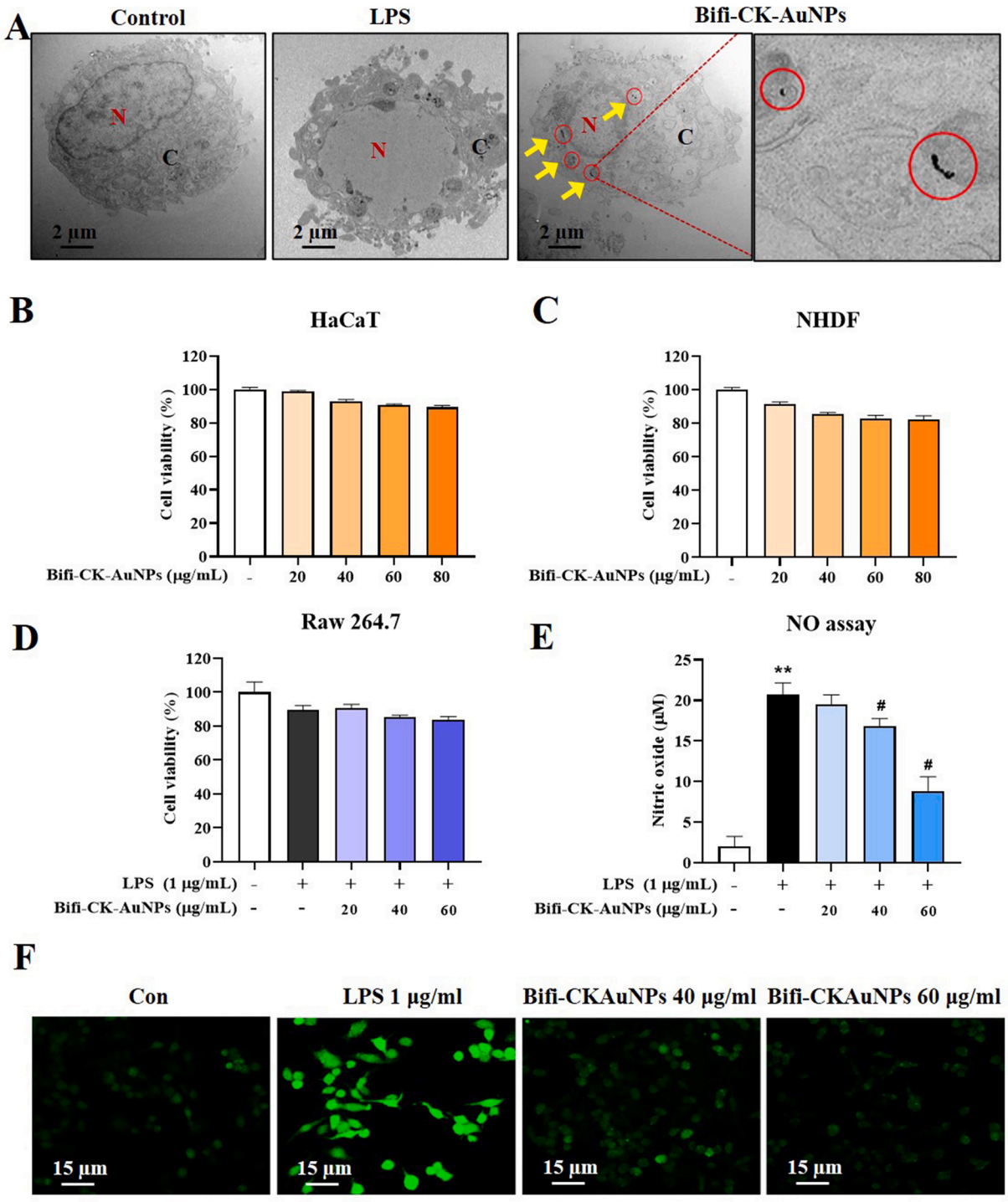

Fig. 3. Intracelluar localization and cell cytotoxicity of Bifi-CKAuNPs. **A.** Bio-TEM images of transport and accumulation of Bifi-CKAuNPs in RAW 264.7 cells; **B & C.** toxicity of Normal skin cells (HaCaTs and NHDFs); **D.** Anti-proliferative activity of Bifi-CKAuNPs in RAW 264.7 cells; **E.** NO assay; **F.** ROS detection with LPS and Bifi-CKAuNPs in RAW 264.7 cells. Densitometry data were expressed as a percentage relative to the untreated control and shown as mean ± SE; $^{*}p < 0.05$, $^{**}p < 0.01$, and $^{***}p < 0.001$ compared to the untreated control; $^{\#}p < 0.05$ compared to the LPS control.

311) (Dhandapani et al., 2023b). The EDX spectrum showed several peaks corresponding to the Au element and with another peak at 8 keV, which can be attributed to the copper grid used for analysis (Fig. 2D) (Dhandapani et al., 2021). Additionally, XRD analysis displayed four distinct peaks for Bifi-CKAuNPs, as depicted in Fig. 2E. These lattice planes were identified as (111, 200, 220, and 311) based on the JCPDS number 00–004–0784 (Jeong et al., 2020). While SAED and XRD are both techniques employed for crystallographic analysis, they differ in the type of radiation used (electrons for SAED, X-rays for XRD) and the scale of analysis (nanoscale for SAED in TEM, broader scale for XRD). The evaluation of Bifi-CKAuNPs stability using Zeta potential yielded a value of −40.33 mV, accompanied by a polydispersity index of 0.10 (Fig. 2F). The negative Zeta potential suggests the presence of a substantial negative surface charge, contributing to the prevention of particle aggregation and precipitation (Serrano-Lotina et al., 2023). Additionally, the low polydispersity index of 0.10 signifies a relatively

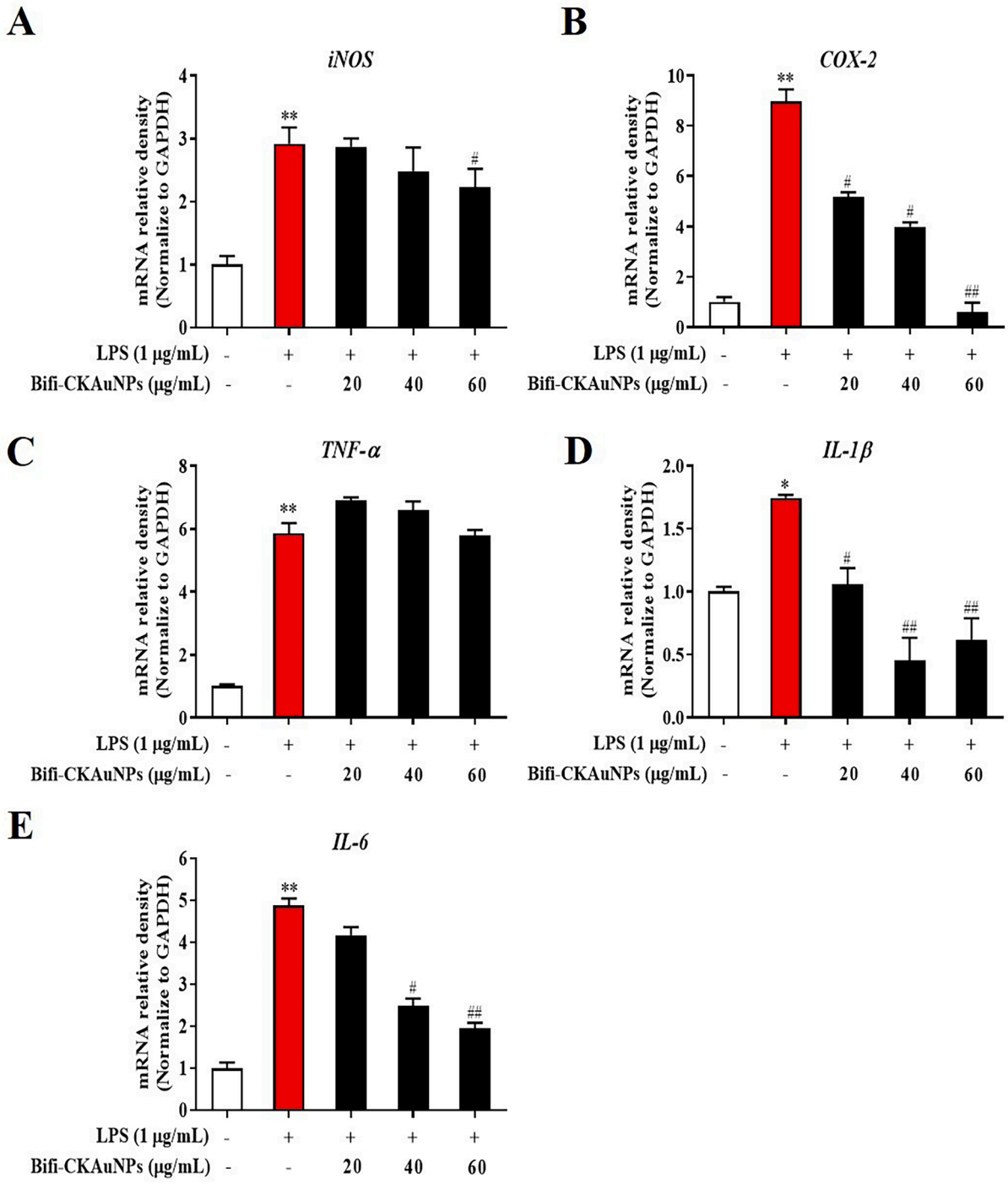

Fig. 4. Effect of Bifi-CKAuNPs on pro-inflammatory mediators and cytokines in RAW 264.7 cells. mRNA expression of **A.** *iNOS*, **B.** *COX-2*, **C.** *TNF-α*, **D.** *IL-1β*, and **E.** *IL-6*, as determined by qRT-PCR and normalized to the corresponding *GAPDH* value. Densitometry data were expressed as a percentage relative to the untreated control and shown as mean ± SE; $^{*}p < 0.05$, $^{**}p < 0.01$, and $^{***}p < 0.001$ compared to the untreated control; $^{\#}p < 0.05$ and $^{\#\#}p < 0.01$, compared to the LPS control.

uniform dispersion, further supporting the conclusion of enhanced stability of Bifi-CKAuNPs in solution. These results indicate that the nanoparticles likely possess favorable stability in the solution. This observed stability is crucial for the effective application of these nanoparticles in biomedical contexts.

Finally, we utilized DLS to assess the average size of the Bifi-CKAuNPs. As illustrated in Fig. 2G, the DLS results indicated an average size of 190 nm. In this study, a notable discrepancy was observed between the nanoscale dimensions measured by DLS and Transmission Electron TEM, with DLS reporting significantly larger particle sizes. This disparity arises from the fact that DLS is applicable for measuring nanoparticles in solution, where potential aggregation or dynamic distribution may lead to an overestimation of particle sizes (Gołębiowski & Buszewski, 2023). In contrast, TEM requires the sample to be prepared in a dried form, typically providing more accurate insights into the actual morphology and size characteristics (Huang et al., 2023b).Taken together, these optimized parameters and physicochemical characterization indicate that Bifi-CKAuNPs were successfully

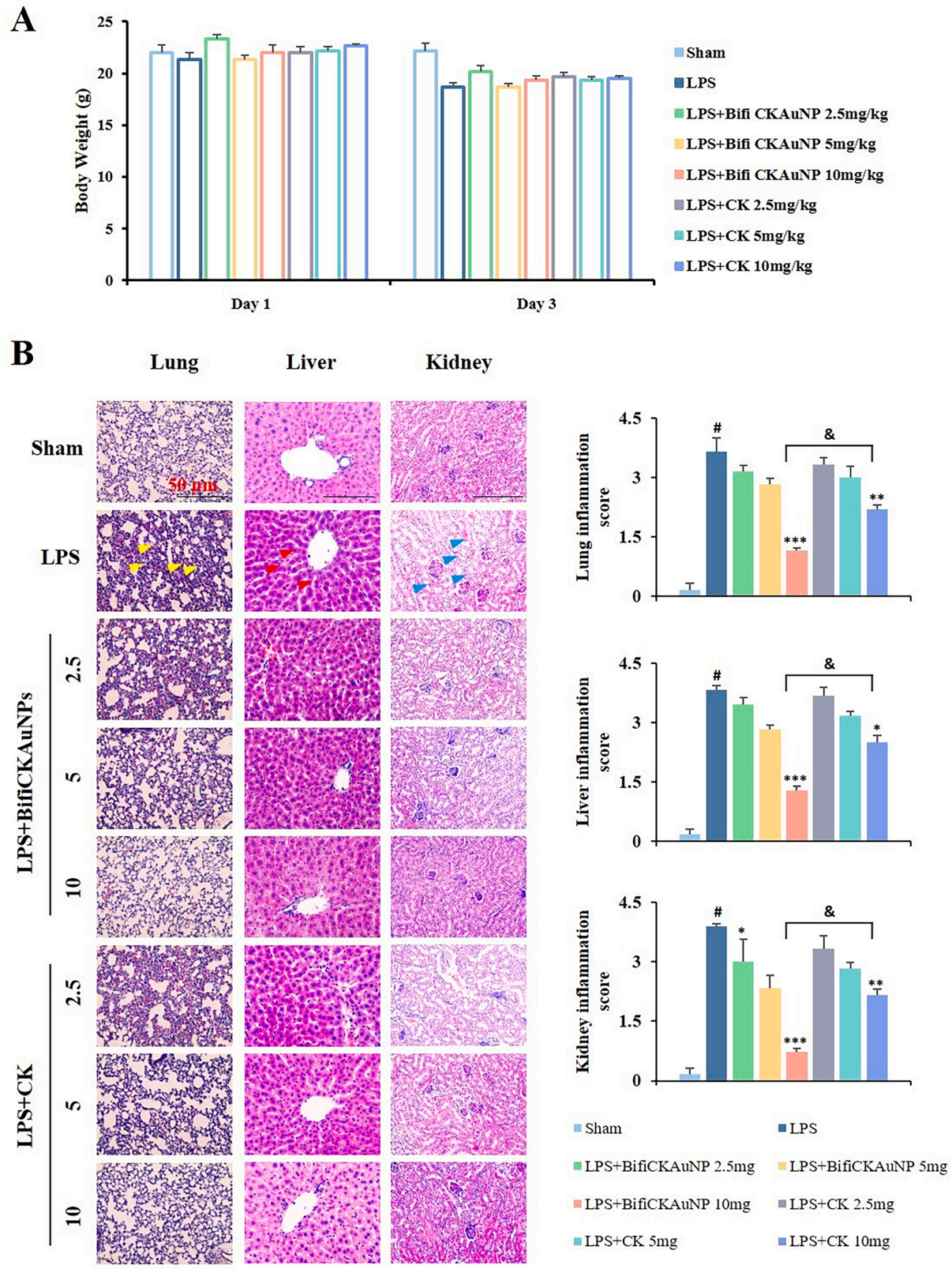

Fig. 5. Effect of Bifi-CKAuNPs on histopathological changes in mice. **A.** Body weight of the mice; **B.** The paraffin sections of the lung (left panel), liver (middle panel), and kidney (right panel) from each group stained with H&E dye; $^{*}p < 0.05$, $^{**}p < 0.01$, and $^{***}p < 0.001$ compared to the LPS group; $^{\#}p < 0.05$, compared to Sham group; $^{\&}p < 0.05$, Bifi-CKAuNPs + LPS group compared to CK + LPS group.

synthesized and are stable.

3.2. Uptake and cytotoxicity of Bifi-CKAuNPs in macrophages

Nanoparticles exhibit the capacity for cellular internalization, a phenomenon facilitated primarily through mechanisms such as endocytosis (de Almeida et al., 2021). This cellular uptake capacity is vital in fields such as nanomedicine for targeted drug delivery. Therefore, internalization of Bifi-CKAuNPs by RAW 264.7 cells was investigated by performing a cell uptake test. The cells were treated for 3 h and analyzed using Bio-TEM. Bifi-CKAuNPs were taken up by the cells through endocytosis, where they were transported into the cytosol via endosomes and lysosomes (Fig. 3A). Unlike the study by Song *et al.* (Song et al., 2013), where AuNPs were observed inside the nucleus, Bifi-CKAuNPs were not detected in the nucleus of RAW 264.7 cells. Instead, they were localized to cell organelles in the cytoplasm.Therefore, this analysis confirmed that endocytosis was the mechanism of internalization. Moreover, it's important to note that the imperative for anti-inflammatory drugs to exhibit non-toxicity towards normal cells arises from the necessity to mitigate inflammation while safeguarding the integrity of healthy tissues. Therefore, the cytotoxicity of Bifi-CKAuNPs was examined by exposing RAW 264.7 cells and normal skin cell lines (NHDFs, HaCaTs) to varying concentrations of Bifi-CKAuNPs (20–80 μg/mL). No significant mortality was observed in the HaCaTs and NHDF cells exposed to Bifi-CKAuNPs (Fig. 3B-C). This observation implies that Bifi-CKAuNPs hold promise as effective and safe targeted nanocarriers. The demonstrated absence of significant cytotoxicity in normal skin cell lines, coupled with successful internalization into inflammatory cells, underscores their potential utility in drug delivery applications for treating inflammatory conditions.

3.3. In vitro anti-inflammatory activity of Bifi-CK-AuNPs

Plant secondary metabolites, including ginsenosides, exhibit anti-inflammatory properties and strongly affect oxidative stress and inflammatory pathways (He et al., 2022). We focused on the effects of Bifi-CKAuNPs on LPS-exposed RAW 264.7 cells treated with 20–80 μg/mL varying concentrations of Bifi-CKAuNPs. NO production and ROS stimulation were assessed as indicators of cytotoxicity and drug efficacy (Fig. 3D and Fig. 3E, respectively). Bifi-CKAuNPs induced a concentration-dependent decrease in NO production in treated cells, thereby suppressing excessive NO expression. Additionally, we examined the capacity of drugs to regulate reactive oxygen species (ROS), which is a multifunctional signaling molecule, in distinct cell types by modulating signaling pathways (Wang et al., 2021). Bifi-CKAuNPs administration resulted in comparable ROS levels between treated and control cells, indicating that Bifi-CKAuNPs inhibited ROS production (Fig. 3F). Therefore, the potential of Bifi-CKAuNPs to regulate ROS and NO levels in cells indicates that they may provide a promising therapeutic option for inflammatory and oxidative-stress-related diseases.

3.4. Molecular detection of gene expression in vitro

Validating the molecular mechanism is crucial for unraveling the intricate cellular and molecular processes influenced by a treatment (Wang et al., 2022). This confirmation yields insights into specific pathways and signaling cascades affected by the treatment, establishing a precise understanding of its effects. In the context of Bifi-CKAuNPs and their down regulate impact on LPS-induced inflammation, we investigated the underlying mechanism of the observed effects of Bifi-CKAuNPs on LPS-induced inflammation by measuring the mRNA expression levels. The pro-inflammatory mediators and cytokines, including inducible nitric oxide synthase (iNOS) (Merenzon et al., 2023), cyclooxygenase-2 (COX-2) (Mohsin & Irfan, 2020), tumor necrosis factor-alpha (TNF-α) (Zhou et al., 2021), interleukin-1 beta (IL-1β) (Cavalli et al., 2021), and interleukin-6 (IL-6) (Hirano, 2021), play crucial roles in immune responses and inflammatory processes. Understanding the intricate functions of these mediators is essential for deciphering immune regulation and developing therapeutic strategies for inflammatory conditions. As shown in Fig. 4, the expression levels of *iNOS, COX-2*, *TNF-α*, *IL-1β*, and *IL-6* cytokines were significantly reduced in LPS-stimulated RAW 246.7 cells after treatment with Bifi-CKAuNPs (20–60 μg/mL). These results indicated that Bifi-CKAuNPs treatment effectively inhibited the expression of proinflammatory cytokines, thereby demonstrating its potential as an anti-inflammatory agent.

3.5. Histopathological observation in mice

The hepatobiliary and renal systems are the primary excretory pathways for drugs and their metabolites (Jetter & Kullak-Ublick, 2020). Drug-induced injury to the liver and kidneys is the predominant cause for the discontinuation of drug discovery research projects (Garcia-Cortes et al., 2020). Although the *in vitro* selective toxicity of Bifi-CKAuNPs towards normal cells has been demonstrated, we investigated the toxicological aspects of Bifi-CKAuNPs and CK to further evaluate their toxic effects. The body weight of sham or LPS-induced mice did not show change significantly during the three-day experiment in any treatment group (Fig. 5A). However, the LPS-treated group exhibited significant pulmonary inflammation, including pulmonary edema, congestion, alveolar hemorrhage, and infiltration into the alveoli and interstitial spaces (Fig. 5B, yellow arrow). In addition, the lung tissue in the LPS-treated group demonstrated a 3.5-fold increase in the inflammation score compared to the sham group. It should be noted that the administration of Bifi-CKAuNPs and CK10 resulted in two-fold to three-fold lower inflammatory changes compared to the LPS group. We conducted several control studies to confirm the anti-inflammatory effects and biosafety of Bifi-CKAuNPs and the results showed that Bifi-CKAuNPs did not cause toxic effects in mice whereas CK10-treatment group existed toxicity on the lung of mice. The hepatic sections of the LPS-treated group exhibited significant histopathological changes, including red blood cell congestion, sinusoidal dilatation, hepatocellular necrosis, and neutrophil infiltration (Fig. 5B, red arrow). However, the administration of Bifi-CKAuNPs resulted in two-fold to three-fold reduction in inflammatory characteristics and scores compared to the LPS-treated and CK 10 + LPS groups. Similarly, the kidney section of the LPS-treated group demonstrated degenerative changes, including vascular edema, capsule cavity swelling, loss of brush borders, extravascular outflow into epithelial cells and tubular space of focal necrosis (Fig. 5B, blue arrow). However, treatment with Bifi-CKAuNPs resulted in two-fold to four-fold reductions in the inflammatory response and score compared to the LPS and LPS + CK groups. Overall, the administration of Bifi-CKAuNPs effectively reduced inflammatory and histological damage in each organ and did not cause toxic effects.

3.6. Inflammatory cytokine protein expression in Bifi-CKAuNPs-treated mice

NF-κB is a transcription factor that controls the expression of various proinflammatory genes and plays a crucial role in regulating inflammatory responses (Dhandapani et al., 2023a; Yi et al., 2023). The activation of NF-κB leads to the production of cytokines, chemokines, and adhesion molecules that recruit immune cells to the site of inflammation, causing tissue damage (Xu et al., 2022). In response to inflammation, p-p38, which is a member of the MAPK family, is activated and promotes the production of pro-inflammatory cytokines (Lauritano et al., 2023). Furthermore, STAT1 and NF-κB demonstrate reciprocal regulation and synergistic interactions, functioning in concert to potentiate the inflammatory cascade by modulating the transcriptional activation of pro-inflammatory genes (Zhang et al., 2021). Therefore, the regulation of these signaling molecules is crucial for controlling inflammation and preventing tissue damage in various inflammatory

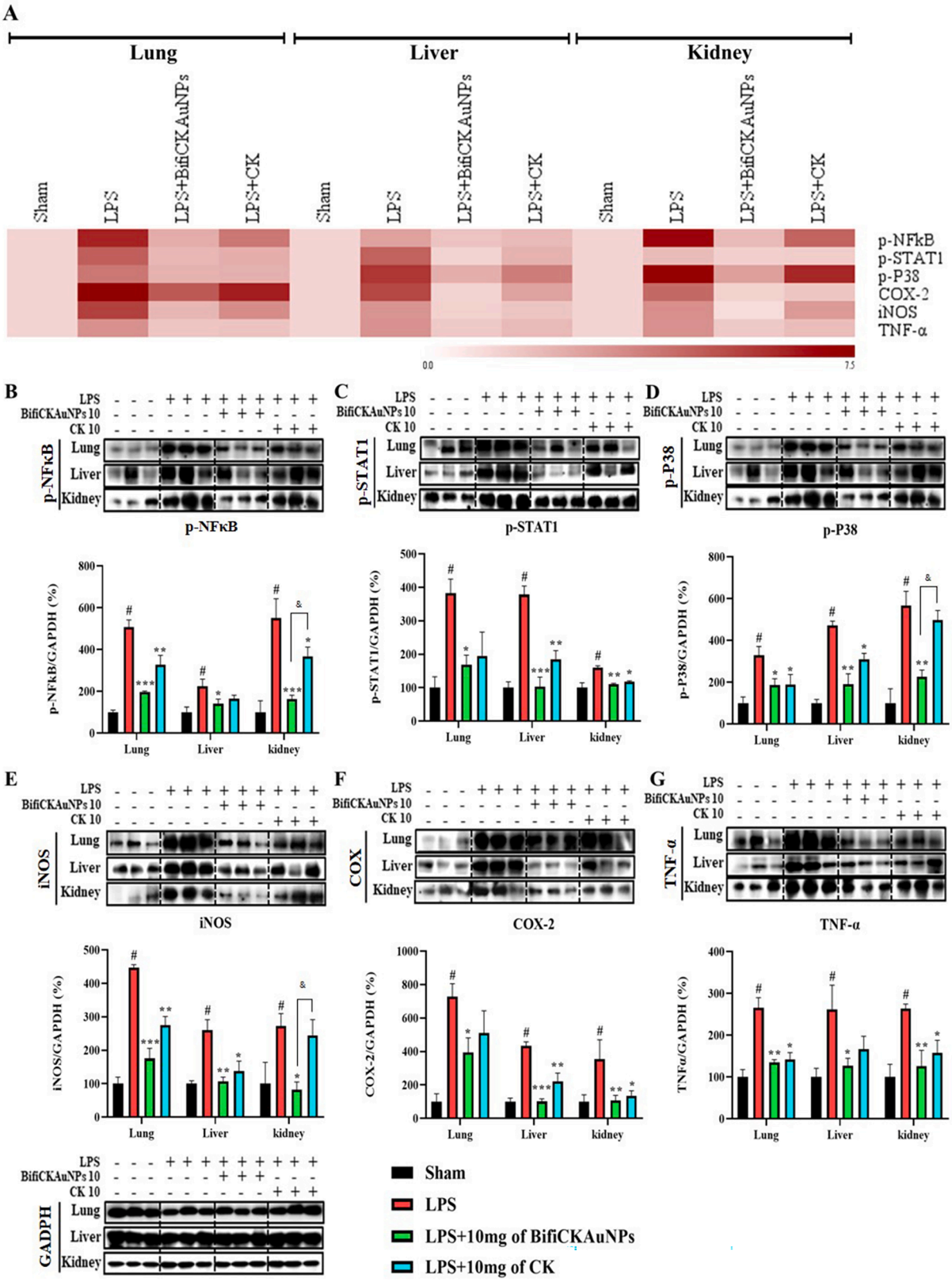

Fig. 6. Effects of Bifi-CKAuNPs on inflammatory mediators in mice. **A.** Heat map analysis of differential expressed proteins; Lysates from the three organs were determined by Western blot analysis and normalized to the corresponding value of GAPDH(B-G); **B.** p-NF-κB, **C.** p-STAT1, **D.** p-P38, **E.** iNOS, **F.** COX-2, and **G.** TNF-α were compared with GAPDH. The result was expressed as the mean ± S; $^{*}p < 0.05$, $^{**}p < 0.01$, and $^{***}p < 0.001$, compared to the LPS group; $^{\#}p < 0.05$, compared to Sham group; $^{\&}p < 0.05$, Bifi-CKAuNPs + LPS group compared to CK + LPS group.

diseases.

A heatmap was used to visualize the expression of inflammation-related proteins in each organ (lungs, liver, kidneys) of the mice (Fig. 6A). LPS-induced mice exhibited significant increases in the levels of the phosphorylated forms of NF-κB, STAT1, and p38 in targeted organs, and in the protein levels of inflammatory mediators (iNOS, COX-2, and TNF-α) in the lungs, liver, and kidneys, as compared to the sham group. The results showed that both Bifi-CKAuNPs and CK exhibit the capacity to mitigate the protein expression of inflammatory mediators in the organs of mice (Fig. 6B). Notably, treatment with Bifi-CKAuNPs was more effective than that with CK. In particular, compared to treatment with CK (10 mg/kg), treatment with Bifi-CKAuNPs (10 mg/kg) significantly reduced the phosphorylated forms protein expression of NF-κB and p38 as well as the inflammatory mediators iNOS in the kidney. These results suggested that Bifi-CKAuNPs protected against acute inflammation in mice by inhibiting LPS-induced inflammatory protein expression. Moreover, although CK originates from the metabolism of a natural product, it has the potential to induce toxicity. Our results indicatded that the use of Bifi-CKAuNPs may be a promising approach for preventing and alleviating disease-causing responses in mouse models compared to the CK. Taken together, our study elucidates the potential mechanisms for improving immune regulation while modulating NF-κB/MAPK signaling pathway. Therefore, Bifi-CKAuNPs was suggested as potential candidates for overcoming the toxicity associated with conventional CK and preventing and improving acute inflammatory diseases by inhibiting NF-κB/ MAPKsignaling pathways.

In a summary, compare to traditional treatment methods utilizing the chemical drug CK, the use of Bifi-CKAuNPs presents a spectrum of potential advantages. The smaller size of Bifi-CKAuNPs contributes to increased bioavailability, facilitating tissue penetration while mitigating adverse effects on non-inflammatory tissues and reducing side effects. However, current research on Bifi-CKAuNPs is limited to preclinical studies. The furture clinical application and scalability issues for large-scale production remain significant challenges. In contrast, traditional treatment methods exhibit broad acceptance and lower production costs, yet may suffer from non-specificity and substantial side-effect. Hence, in the process of selecting a treatment approach, it is imperative to comprehensively consider disease characteristics and therapeutic objectives to attain an optimal balance.

4. Conclusions

In this study, we developed a cost-effective method for the biogenic synthesis of gold nanoparticles loaded with ginsenoside CK using probiotic bacteria. We hypothesized that Bifi-CK-AuNPs might possess anti-inflammatory properties, and to test this hypothesis, we evaluated their efficacy in LPS-stimulated RAW 264.7 cells and a mouse model of LPS-induced inflammation. The results demonstrated that Bifi-CK-AuNPs exhibited minimal cytotoxicity while significantly reducing LPS-induced NO and ROS production, along with decreased mRNA expression of pro-inflammatory cytokines in cells. Molecular analysis revealed the inhibition of the NF-κB signaling pathway. Overall, this study highlights the potential of probiotic-synthesized AuNPs as drug delivery carriers and emphasizes the applications of Bifi-CK-AuNPs in anti-inflammatory drug development, providing a foundation for further exploration in various biological contexts. Furthermore, for the extensive industrial utilization of Bifi-CKAuNPs, it is essential to undertake additional investigations, encompassing clinical trials, to thoroughly examine their impact on human health, with a particular emphasis on safety considerations. These inquiries will be undertaken in our forthcoming research.

CRediT authorship contribution statement

Seunghyun Kim: Data curation, Writing – original draft. **Rongbo Wang:** Data curation, Writing – original draft. **Sanjeevram Dhandapani:** . **Kyungsu Kang:** Data curation. **Ik-Hyun Cho:** Supervision. **Yeon-Ju Kim:** Supervision.

Declaration of competing interest

The authors declare that they have no known competing financial interests or personal relationships that could have appeared to influence the work reported in this paper.

Acknowledgments

This work was supported by KDBIO Corp. and also supported by the fund “National Research Foundation of Korea (2023R1A2C1007606/NRF-2022R1A2C2009817) and also supported by the fund “Cooperative Research Program for Agriculture Science and Technology Development (PJ01703502)” Rural Development Administration, Republic of Korea. We would like to extend our sincere appreciation to Mr. Bum min Chon, Kyung Hee University for their invaluable technical assistance throughout the course of histopathological analysis.

Appendix A. Supplementary data

Supplementary data to this article can be found online at https://doi.org/10.1016/j.arabjc.2024.105650.

References

Abdelkawi, A., Slim, A., Zinoune, Z., Pathak, Y., 2023. Surface modification of metallic nanoparticles for targeting drugs. Coatings 13 (9), 1660.
Ahmad, S.S., Ahmad, K., Hwang, Y.C., Lee, E.J., Choi, I., 2023. Therapeutic applications of ginseng natural compounds for health management. Int. J. Mol. Sci. 24 (24), 17290.
Amini, Y., Hassanvand, A., Ghazanfari, V., Shadman, M.M., Heydari, M., Alborzi, Z.S., 2023. Optimization of liquid-liquid extraction of calcium with a serpentine microfluidic device. Int. Commun. Heat Mass Transfer 140, 106551.
Awasthi, A.K., Gupta, S., Namdev, K.R., Banerjee, A., Srivastava, A., 2021. Polydopamine and dopamine interfere with tetrazolium-based cytotoxicity assays and produce exaggerated cytocompatibility inferences. Biomater. Sci. 9 (9), 3300–3305.
Balusamy, S.R., Karuppieh, S., Venkat, S., Thangavelu, L., Kim, Y.J., Perumalsamy, H., 2022. Biomedical applications of ginsenosides nanoparticles synthesized using microbes. In: Agri-Waste and Microbes for Production of Sustainable Nanomaterials. Elsevier, pp. 625–653.
Borse, V.B., Konwar, A.N., Jayant, R.D., Patil, P.O., 2020. Perspectives of characterization and bioconjugation of gold nanoparticles and their application in lateral flow immunosensing. Drug Deliv. Transl. Res. 10, 878–902.
Cavalli, G., Colafrancesco, S., Emmi, G., Imazio, M., Lopalco, G., Maggio, M.C., Sota, J., Dinarello, C.A., 2021. Interleukin 1α: a comprehensive review on the role of IL-1α in the pathogenesis and treatment of autoimmune and inflammatory diseases. Autoimmun. Rev. 20 (3), 102763.
Choi, J.H., Lee, M.J., Jang, M., Kim, H.-J., Lee, S., Lee, S.W., Kim, Y.O., Cho, I.-H., 2018. Panax ginseng exerts antidepressant-like effects by suppressing neuroinflammatory response and upregulating nuclear factor erythroid 2 related factor 2 signaling in the amygdala. J. Ginseng Res. 42 (1), 107–115.
Cong, L., Ma, J., Zhang, Y., Zhou, Y., Cong, X., Hao, M., 2023. Effect of anti-skin disorders of ginsenosides-A Systematic Review. J. Ginseng Res.
de Almeida, M.S., Susnik, E., Drasler, B., Taladriz-Blanco, P., Petri-Fink, A., Rothen-Rutishauser, B., 2021. Understanding nanoparticle endocytosis to improve targeting strategies in nanomedicine. Chem. Soc. Rev. 50 (9), 5397–5434.
Dhandapani, S., Xu, X., Wang, R., Puja, A.M., Kim, H., Perumalsamy, H., Balusamy, S.R., Kim, Y.-J., 2021. Biosynthesis of gold nanoparticles using Nigella sativa and Curtobacterium proimmune K3 and evaluation of their anticancer activity. Mater. Sci. Eng. C 127, 112214.
Dhandapani, S., Wang, R., Cheol Hwang, K., Kim, H., Kim, Y.-J., 2023a. Enhanced skin anti-inflammatory and moisturizing action of gold nanoparticles produced utilizing Diospyros kaki fruit extracts. Arab. J. Chem. 16 (4), 104551.
Dhandapani, S., Wang, R., Cheol Hwang, K., Kim, H., Kim, Y.-J., 2023b. Exploring the potential anti-inflammatory effect of biosynthesized gold nanoparticles using Isodon excisus leaf tissue in human keratinocytes. Arab. J. Chem. 16 (10), 105113.
Falahati, M., Attar, F., Sharifi, M., Saboury, A.A., Salihi, A., Aziz, F.M., Kostova, I., Burda, C., Priecel, P., Lopez-Sanchez, J.A., 2020. Gold nanomaterials as key suppliers in biological and chemical sensing, catalysis, and medicine. Biochim. Biophys. Acta (BBA)-Gen. Subj. 1864 (1), 129435.
Garcia-Cortes, M., Robles-Diaz, M., Stephens, C., Ortega-Alonso, A., Lucena, M.I., Andrade, R.J., 2020. Drug induced liver injury: an update. Arch. Toxicol. 94, 3381–3407.
Gavilán, H., Serrano, M.B., Cabanelas, J.C., 2023. Nanomaterials and their synthesis for a sustainable future. New Mater. Circul. Econ. 149, 233–310.

Gołębiowski, A., Buszewski, B., 2023. Characterization of colloidal particles of a biological and metallic nature. Microchem. J. 108864.
Guo, L., Li, T., Guo, G., Liu, Z., Hao, N., 2023. The synthesis of ginsenoside compound K using a surface-displayed β-glycosidase whole-cell catalyst. Catalysts 13 (10), 1375.
Hammami, I., Alabdallah, N.M., 2021. Gold nanoparticles: Synthesis properties and applications. J. King Saud Univ. Sci. 33 (7), 101560.
Hassan, H., Sharma, P., Hasan, M.R., Singh, S., Thakur, D., Narang, J., 2022. Gold nanomaterials–The golden approach from synthesis to applications. Mater. Sci. Energy Technol.
He, B., Chen, D., Zhang, X., Yang, R., Yang, Y., Chen, P., Shen, Z., 2022. Oxidative stress and ginsenosides: An update on the molecular mechanisms. Oxidative Med Cell. Long. 2022.
Hirano, T., 2021. IL-6 in inflammation, autoimmunity and cancer. Int. Immunol. 33 (3), 127–148.
Hou, M., Wang, R., Zhao, S., Wang, Z., 2021. Ginsenosides in Panax genus and their biosynthesis. Acta Pharm. Sin. B 11 (7), 1813–1834.
Huang, Y., Chen, Q., Zeng, H., Yang, C., Wang, G., Zhou, L., 2023b. A review of selenium (Se) nanoparticles: from synthesis to applications. Part. Part. Syst. Char. 40 (11), 2300098.
Huang, S., Yuan, J., Xie, Y., Qing, K., Shi, Z., Chen, G., Gao, J., Tan, H., Zhou, W., 2023a. Targeting nano-regulator based on metal–organic frameworks for enhanced immunotherapy of bone metastatic prostate cancer. Cancer Nanotechnol. 14 (1), 1–15.
Jeong, S., Liu, Y., Zhong, Y., Zhan, X., Li, Y., Wang, Y., Cha, P.M., Chen, J., Ye, X., 2020. Heterometallic seed-mediated growth of monodisperse colloidal copper nanorods with widely tunable plasmonic resonances. Nano Lett. 20 (10), 7263–7271.
Jetter, A., Kullak-Ublick, G.A., 2020. Drugs and hepatic transporters: A review. Pharmacol. Res. 154, 104234.
Kumari, V., Vishwas, S., Kumar, R., Kakoty, V., Khursheed, R., Babu, M.R., Harish, V., Mittal, N., Singh, P.K., Alharthi, N.S., 2023. Anoverview of biomedical applications for gold nanoparticles against lung cancer. J. Drug Delivery Sci. Technol. 104729.
Lapresta-Fernández, A., Fernández, A., Blasco, J., 2012. Nanoecotoxicity effects of engineered silver and gold nanoparticles in aquatic organisms. TrAC Trends Anal. Chem. 32, 40–59.
Lauritano, D., Mastrangelo, F., D'Ovidio, C., Ronconi, G., Caraffa, A., Gallenga, C.E., Frydas, I., Kritas, S.K., Trimarchi, M., Carinci, F., 2023. Activation of Mast Cells by Neuropeptides: The Role of Pro-Inflammatory and Anti-Inflammatory Cytokines. Int. J. Mol. Sci. 24 (5), 4811.
Liu, Y., Perumalsamy, H., Kang, C.H., Kim, S.H., Hwang, J.-S., Koh, S.-C., Yi, T.-H., Kim, Y.-J., 2020. Intracellular synthesis of gold nanoparticles by Gluconacetobacter liquefaciens for delivery of peptide CopA3 and ginsenoside and anti-inflammatory effect on lipopolysaccharide-activated macrophages. Artif. Cells Nanomed. Biotechnol. 48 (1), 777–788.
Marsousi, S., Karimi-Sabet, J., Moosavian, M.A., Amini, Y., 2019. Liquid-liquid extraction of calcium using ionic liquids in spiral microfluidics. Chem. Eng. J. 356, 492–505.
Merenzon, M.A., Arias, E.H., Bhatia, S., Shah, A.H., Higgins, D.M., Villaverde, M., Belgorosky, D., Eijan, A.M., 2023. Nitric oxide synthase inhibitors as potential therapeutic agents for gliomas: A systematic review. Nitric Oxide.
Mikhailova, E.O., 2021. Gold nanoparticles: biosynthesis and potential of biomedical application. J. Funct. Biomater. 12 (4), 70.
Mills, J.A., Liu, F., Jarrett, T.R., Fletcher, N.L., Thurecht, K.J., 2022. Nanoparticle based medicines: approaches for evading and manipulating the mononuclear phagocyte system and potential for clinical translation. Biomater. Sci. 10 (12), 3029–3053.
Mohsin, N.-U.-A., Irfan, M., 2020. Selective cyclooxygenase-2 inhibitors: A review of recent chemical scaffolds with promising anti-inflammatory and COX-2 inhibitory activities. Med. Chem. Res. 29, 809–830.
Nejati, K., Dadashpour, M., Gharibi, T., Mellatyar, H., Akbarzadeh, A., 2021. Biomedical applications of functionalized gold nanoparticles: a review. J. Clust. Sci. 1–16.
Paul, T.K., Jalil, M.A., Repon, M.R., Alim, M.A., Islam, T., Rahman, S.T., Paul, A., Rhaman, M., 2023. Mapping the Progress in Surface Plasmon Resonance Analysis of Phytogenic Silver Nanoparticles with Colorimetric Sensing Applications. Chem. Biodivers. 20 (8), e202300510.
Potenza, M.A., Montagnani, M., Santacroce, L., Charitos, I.A., Bottalico, L., 2023. Ancient herbal therapy: A brief history of Panax ginseng. J. Ginseng Res. 47 (3), 359–365.
Radulescu, D.-M., Surdu, V.-A., Ficai, A., Ficai, D., Grumezescu, A.-M., Andronescu, E., 2023. Green synthesis of metal and metal oxide nanoparticles: a review of the principles and biomedical applications. Int. J. Mol. Sci. 24 (20), 15397.
Ratan, Z.A., Haidere, M.F., Hong, Y.H., Park, S.H., Lee, J.-O., Lee, J., Cho, J.Y., 2021. Pharmacological potential of ginseng and its major component ginsenosides. J. Ginseng Res. 45 (2), 199–210.
Sadeghi, A., Amini, Y., Saidi, M.H., Yavari, H., 2015. Shear-rate-dependent rheology effects on mass transport and surface reactions in biomicrofluidic devices. AIChE J 61 (6), 1912–1924.
Sanità, G., Carrese, B., Lamberti, A., 2020. Nanoparticle surface functionalization: how to improve biocompatibility and cellular internalization. Front. Mol. Biosci. 7, 587012.
Sarani, M., Roostaee, M., Adeli-Sardou, M., Kalantar-Neyestanaki, D., Mousavi, S.A.A., Amanizadeh, A., Barani, M., Amirbeigi, A., 2024. Green synthesis of Ag and Cu-doped Bismuth oxide nanoparticles: Revealing synergistic antimicrobial and selective cytotoxic potentials for biomedical advancements. J. Trace Elem. Med Biol. 81, 127325.
Sarhene, M., Ni, J.Y., Duncan, E.S., Liu, Z., Li, S., Zhang, J., Guo, R., Gao, S., Gao, X., Fan, G., 2021. Ginsenosides for cardiovascular diseases; update on pre-clinical and clinical evidence, pharmacological effects and the mechanisms of action. Pharmacol. Res. 166, 105481.
Serrano-Lotina, A., Portela, R., Baeza, P., Alcolea-Rodriguez, V., Villarroel, M., Ávila, P., 2023. Zeta potential as a tool for functional materials development. Catal. Today 423, 113862.
Sharma, A., Lee, H.-J., 2020. Ginsenoside compound K: Insights into recent studies on pharmacokinetics and health-promoting activities. Biomolecules 10 (7), 1028.
Shen, W., Pei, P., Zhang, C., Li, J., Han, X., Liu, T., Shi, X., Su, Z., Han, G., Hu, L., 2023. A polymeric hydrogel to eliminate programmed death-ligand 1 for enhanced tumor radio-immunotherapy. ACS Nano 17 (23), 23998–24011.
Song, K., Xu, P., Meng, Y., Geng, F., Li, J., Li, Z., Xing, J., Chen, J., Kong, B., 2013. Smart gold nanoparticles enhance killing effect on cancer cells. Int J Oncol 42 (2), 597–608.
Sreedharan, S.M., Gupta, S., Saxena, A.K., Singh, R., 2019. Macrophomina phaseolina: microbased biorefinery for gold nanoparticle production. Ann. Microbiol. 69, 435–445.
Tam, D.N.H., Nam, N.H., Cuong, N.T.K., Hung, D.T., Soa, D.T., Altom, A., Tran, L., Elhadad, H., Huy, N.T., 2023. Compound K: A systematic review of its anticancer properties and probable mechanisms. Fundam. Clin. Pharmacol.
Wang, R., Moon, S.-K., Kim, W.-J., Dhandapani, S., Kim, H., Kim, Y.-J., 2022. Biologically synthesized Rosa rugosa-based gold nanoparticles suppress skin inflammatory responses via MAPK and NF-κB Signaling pathway in TNF-α/IFN-γ-induced HaCaT keratinocytes. ACS Omega 7 (40), 35951–35960.
Wang, L., Quine, S., Frickenstein, A.N., Lee, M., Yang, W., Sheth, V.M., Bourlon, M.D., He, Y., Lyu, S., Garcia-Contreras, L., 2023a. Exploring and analyzing the systemic delivery barriers for nanoparticles. Adv. Funct. Mater. 2308446.
Wang, J., Sun, D., Huang, L., Wang, S., Jin, Y., 2021. Targeting reactive oxygen species capacity of tumor cells with repurposed drug as an anticancer therapy. Oxidative Med Cell Long. 2021.
Wang, Y., Zhai, W., Cheng, S., Li, J., Zhang, H., 2023b. Surface-functionalized design of blood-contacting biomaterials for preventing coagulation and promoting hemostasis. Friction 1–24.
Wen, C., Wang, L., Liu, L., Shen, X.C., Chen, H., 2022. Surface-enhanced raman probes based on gold nanomaterials for in vivo diagnosis and imaging. Chem. Asian J. 17 (7), e202200014.
Xu, X.Y., Dhandapani, S., Mi, X.J., Park, H.-R., Kim, Y.-J., 2022. Immune-enhancing efficacy of Curtobacterium proimmune K3 lysates isolated from Panax ginseng beverages in cyclophosphamide-induced immunosuppressed mice. J. Funct. Foods 92, 105020.
Yi, J., Li, L., Yin, Z.-J., Quan, Y.-Y., Tan, R.-R., Chen, S.-L., Lang, J.-R., Li, J., Zeng, J., Li, Y., 2023. Polypeptide from moschus suppresses lipopolysaccharide-induced inflammation by inhibiting NF-κ B-ROS/NLRP3 pathway. Chin. J. Integr. Med. 29 (10), 895–904.
Yu, W., Zhang, T., Ma, M., Chen, C., Liang, X., Wen, K., Wang, Z., Shen, J., 2018. Highly sensitive visual detection of amantadine residues in poultry at the ppb level: A colorimetric immunoassay based on a Fenton reaction and gold nanoparticles aggregation. Anal. Chim. Acta 1027, 130–136.
Zeng, J., Zhang, Y., Zeng, T., Aleisa, R., Qiu, Z., Chen, Y., Huang, J., Wang, D., Yan, Z., Yin, Y., 2020. Anisotropic plasmonic nanostructures for colorimetric sensing. Nano Today 32, 100855.
Zhang, D., Ma, X.-L., Gu, Y., Huang, H., Zhang, G.-W., 2020. Green synthesis of metallic nanoparticles and their potential applications to treat cancer. Front. Chem. 8.
Zhang, T., Ma, C., Zhang, Z., Zhang, H., Hu, H., 2021. NF-κB signaling in inflammation and cancer. MedComm 2 (4), 618–653.
Zhou, Y., Fan, R., Botchway, B.O., Zhang, Y., Liu, X., 2021. Infliximab can improve traumatic brain injury by suppressing the tumor necrosis factor alpha pathway. Mol. Neurobiol. 58, 2803–2811.
Zhou, L., Li, Z.K., Li, C.Y., Liang, Y.Q., Yang, F., 2022. Anticancer properties and pharmaceutical applications of ginsenoside compound K: A review. Chem. Biol. Drug Des. 99 (2), 286–300.
Zou, L., Shen, R., Ling, L., Li, G., 2018. Sensitive DNA detection by polymerase chain reaction with gold nanoparticles. Anal. Chim. Acta 1038, 105–111.